

Engineering rich two-dimensional higher-order topological phases by flux and periodic driving

Ming-Jian Gao¹ and Jun-Hong An^{1,*}

¹Key Laboratory of Quantum Theory and Applications of MoE, Lanzhou Center for Theoretical Physics, and Key Laboratory of Theoretical Physics of Gansu Province, Lanzhou University, Lanzhou 730000, China

Nodal-line semimetal is commonly believed to exist in \mathcal{PT} symmetric or mirror-rotation symmetric systems. Here, we find a flux-induced parameter-dimensional second-order nodal-line semimetal (SONLS), which has the coexisting hinge Fermi arcs and drumhead surface states, in a two-dimensional system without \mathcal{PT} and mirror-rotation symmetries. Meanwhile, we discover a flux-induced second-order topological insulator (SOTI). Then we artificially create exotic hybrid-order nodal-line semimetals with fruitful nodal-line structures hosted by different quasienergy gaps and widely tunable numbers of corner states by applying a periodic driving on our SONLS and SOTI, respectively. Such Floquet engineered high tunability of the orders and the nodal-line structures of the SONLS and the corner-state number of SOTI sets up a foundation on exploring their further applications.

Introduction.—As one of the most actively expanding fields in physics, topological phases of matter not only enrich the paradigm of condensed matter physics, but also have profound impacts on quantum technologies [1–5]. Featuring as the unique Fermi arc and gapless bulk band, Dirac [6–14], Weyl [15–23], and nodal-line [24–29] semimetals have attracted much attention. They have exhibited their ability in designing topological devices by using their chiral-anomaly induced giant magnetoresistance and high carrier mobility [30–33]. Because of their potential applications in semiconductor integrated circuits, the 2D topological semimetals are also widely studied [34–36]. The finding of higher-order topological phases opens up a new frontier of topological physics [37–55]. Second-order topological insulators (SOTI) are characterized by corner in two-dimension (2D) or hinge states in three-dimension (3D) systems and have some fantastic applications [56]. Second-order nodal-line semimetals (SONLS) with coexisting hinge Fermi arcs and drumhead surface states [52–54] have also been predicted. Yet, the general ways of inducing SONLS and SOTI are scarce.

Symmetries play a leading role in classifying topological phases. Dirac semimetals present in systems with spatial inversion \mathcal{P} and time-reversal \mathcal{T} symmetries. If either of the two symmetries is broken, then Weyl semimetals may be formed. Nodal-line semimetals are thought to present in systems with \mathcal{PT} or mirror-rotation symmetry [57]. SONLS were predicted in \mathcal{PT} symmetric systems [51–53] and mirror-rotation symmetric systems [54]. An open question is whether these symmetries are a prerequisite for SONLS. On the other hand, one of the difficulties in the application of topological phases is that the control ways to various of interactions in natural materials are limited because their features would not be switched anymore once they are fabricated. Coherent control via periodic driving of external fields dubbed Floquet engineering has become a versatile tool in creating novel topological phases in systems of ultracold atoms [58, 59], photonics [60], superconductor qubits [61]. Many exotic

phases absent in static systems have been controllably generated by periodic driving [62–71]. A natural question is that can we realize a free tunability and conversion of the nodal-line structures and the topological phases of a SONLS and SOTI by Floquet engineering.

Addressing on these questions, we here investigate the flux-induced higher-order 2D topological phases and its Floquet engineering. A parameter-dimensional SONLS induced by a flux, with the third dimension simulated by one system parameter, is discovered in our 2D system with neither \mathcal{PT} nor mirror-rotation symmetries. Enriching the family of 2D topological phases, this exotic phase can be readily generalized to the 3D case. We also find a flux-induced SOTI as a byproduct. We further reveal the wide tunability of the nodal-line structures and the topological phases of the SONLS and SOTI by Floquet engineering. Hybrid-order nodal-line semimetal, fruitful nodal-line structures, and exotic topological phases with a widely tunable numbers of zero- and π/T -mode corner states are created at ease by applying a periodic driving. Our work highlights the flux and Floquet engineering as two convenient ways to control and explore novel higher-order topological phases.

Flux-induced second-order topological phases.—Conventionally, nodal-line semimetal exists in the systems with either \mathcal{PT} symmetry or mirror-rotation symmetry [57]. We explore whether these symmetries are the prerequisite of forming nodal-line semimetal. For this purpose, we consider a system of spinless fermions moving on a square lattice, see Fig. 1(a). Its momentum-space Hamiltonian reads $\hat{H} = \sum_{\mathbf{k}} \hat{C}_{\mathbf{k}}^\dagger [\mathcal{H}_0(\mathbf{k}) + \mathcal{H}_1(\mathbf{k})] \hat{C}_{\mathbf{k}}$ with $\hat{C}_{\mathbf{k}}^\dagger = (\hat{C}_{\mathbf{k},1}^\dagger \ \hat{C}_{\mathbf{k},2}^\dagger \ \hat{C}_{\mathbf{k},3}^\dagger \ \hat{C}_{\mathbf{k},4}^\dagger)$ and

$$\mathcal{H}_j(\mathbf{k}) = \begin{pmatrix} 0 & d_j(\mathbf{k}) \\ d_j^\dagger(\mathbf{k}) & 0 \end{pmatrix}, \quad (j = 0, 1), \quad (1)$$

where $d_0(\mathbf{k}) = (\gamma_x + \lambda \cos k_x)\tau_0 - i\lambda \sin k_x \tau_x - i(\gamma_y + \lambda \cos k_y)\tau_y + i\lambda \sin k_y \tau_z$, with τ_i being Pauli matrices and τ_0 being identity matrix. $\gamma_{x/y}$ is the intercell hop-

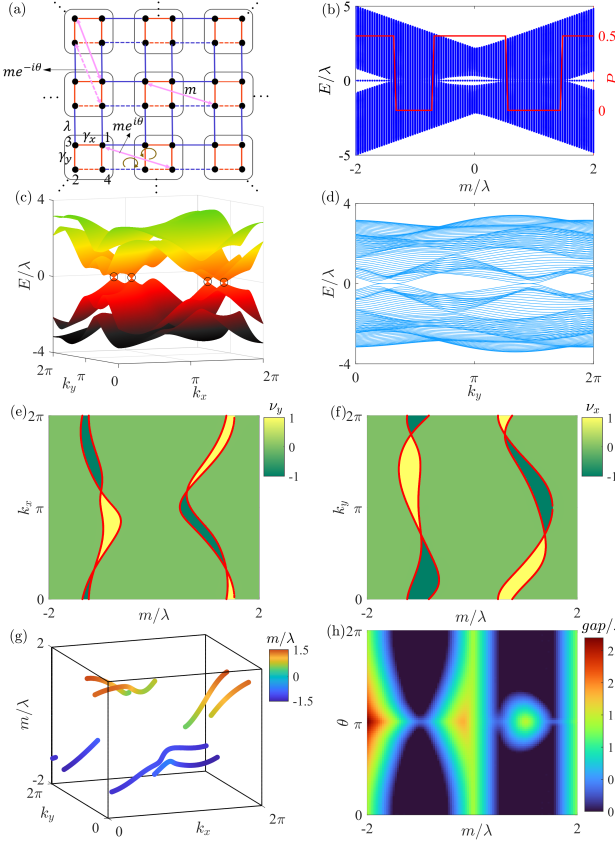


FIG. 1. (a) Scheme of our system. $\gamma_{x/y}$ and λ are the intracell and nearest-neighbor intercell hopping rates, m is the third-order neighbor intercell one, and θ is the flux-induced Peierls phase. The dashed lines denote the hopping rates with a π -phase difference from their solid counterparts. (b) Energy spectrum and quadrupole moment (red line) as a function of m . Energy spectra (c) in momentum space and (d) under the x -direction open boundary condition when $m = 1$. Chiral winding numbers $\nu_{x/y}$ and nodal lines (in red lines) in the (e) k_x - m and (f) k_y - m planes. (g) Nodal lines in the Brillouin zone. (h) Phase diagram described by the bulk gap. We use $\gamma_x = 0.65\lambda$, $\gamma_y = -0.4\lambda$, and $\theta = \pi/2$.

ping rate and λ is the nearest-neighbor intercell hopping rate. Being the Benalcazar-Bernevig-Hughes model, the system described by $\mathcal{H}_0(\mathbf{k})$ has the chiral symmetry $\mathcal{S} = \tau_z \sigma_0$, \mathcal{PT} symmetry, and mirror-rotation symmetry and is a SOTI when $|\gamma_x| < |\lambda|$ and $|\gamma_y| < |\lambda|$ [72]. Inspired by the flux-induced topological phase transition [73], we apply a flux to break the \mathcal{PT} and mirror-rotation symmetries of $\mathcal{H}_0(\mathbf{k})$. The minimal allowable hopping to make the overall flux of the lattice be zero [74] is the third-order neighbor intercell hopping with $d_1(\mathbf{k}) = m[e^{i(\theta+k_x)}(\tau_x + i\tau_y) + e^{-ik_x}(\tau_x - i\tau_y)]/2 + m[e^{i(\theta-k_y)}(\tau_z - \tau_0) + e^{ik_y}(\tau_0 + \tau_z)]/2$, where m is the third-order neighbor intercell hopping rate and θ is the corresponding Peierls phase induced by the flux. Only the chiral symmetry is present in $\mathcal{H}(\mathbf{k}) = \mathcal{H}_0(\mathbf{k}) + \mathcal{H}_1(\mathbf{k})$.

It is interesting to find that a parameter-dimensional

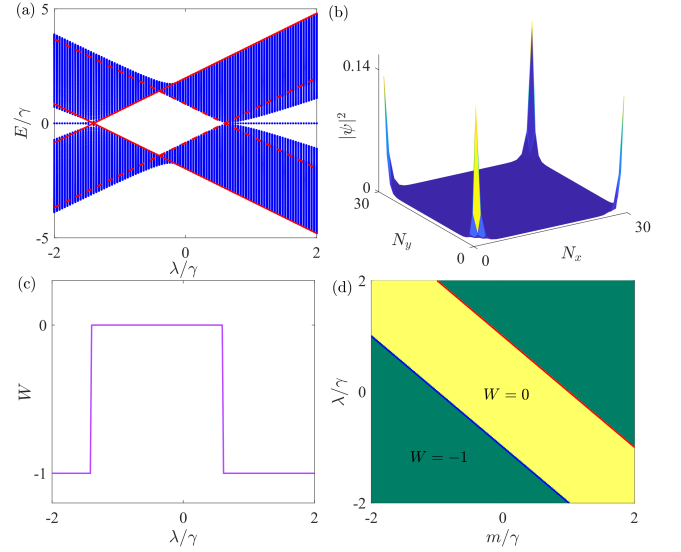


FIG. 2. (a) Energy spectrum and (c) mirror-graded winding number W as a function of λ when $m = 0.4\gamma$. The red solid (dashed) line is the dispersion relation along the high-symmetry line $k = 0$ (π). (b) Probability distribution of the zero-mode state. (d) Phase diagram described by W . We use $\theta = \pi$.

SONLS, where m is seen as an addition dimension besides $k_{x/y}$, is formed in our system with neither \mathcal{PT} symmetry nor the mirror-rotation symmetry in the $\gamma_x \neq \gamma_y$ regime. The second-order topology is characterized by the quadrupole moment $P = [\frac{\text{Im} \ln \det \mathcal{U}}{2\pi} - \sum_{\mathbf{n}, i; \mathbf{m}, j} \frac{X_{\mathbf{n}, i; \mathbf{m}, j}}{2L_x L_y}] \bmod 1$. Here the elements read $\mathcal{U}_{ab} \equiv \langle \psi_a | e^{i2\pi X/(L_x L_y)} | \psi_b \rangle$, $|\psi_\alpha\rangle$ ($\alpha = a, b$) satisfying $\hat{H}|\psi_\alpha\rangle = E_\alpha|\psi_\alpha\rangle$ and $E_\alpha < 0$ are the occupied eigen states, and the coordinate $X_{\mathbf{n}, i; \mathbf{m}, j} = n_x n_y \delta_{\mathbf{n}\mathbf{m}} \delta_{ij}$ with $i, j = 1, \dots, 4$ being the sublattices and $n_{x,y}$ being the numbers of unit cell [75, 76]. The energy spectrum under the open boundary condition in Fig. 1(b) shows that fourfold degenerate zero-mode corner states signified by $P = 0.5$ are formed. In the band-closing parameter regime with $P = 0$, the dispersion relation exhibits four Weyl points, see Fig. 1(c). Its corresponding energy spectrum in the y -direction periodic boundary condition reveals that a flat band is present between each pair of Weyl points, see Fig. 1(d). It is remarkable to find that the flat band is nontrivial in first-order topology, which can be characterized by the winding number [3, 77]

$$\nu_p = \frac{1}{4\pi i} \int_{-\pi}^{\pi} \text{Tr}[\mathcal{S} \mathcal{Q}(\mathbf{k}) \partial_{k_p} \mathcal{Q}(\mathbf{k})] dk_p. \quad (2)$$

Here $p = x, y$ and $\mathcal{Q}(\mathbf{k}) = \sum_{l=1,2} [|u_{-l}(\mathbf{k})\rangle \langle u_{-l}(\mathbf{k})| - |u_l(\mathbf{k})\rangle \langle u_l(\mathbf{k})|]$, with $|u_l(\mathbf{k})\rangle$ satisfying $\mathcal{H}(\mathbf{k})|u_l(\mathbf{k})\rangle = E_l(\mathbf{k})|u_l(\mathbf{k})\rangle$. Figures 1(e) and 1(f) indicate that the band-closing regimes in Fig. 1(b) hold nontrivial first-order topology, whose boundaries form the nodal lines. Separating the first- and second-order phases, such nodal

lines are in the second-order type, whose distribution in the m -parameterized Brillouin zone is shown in Fig. 1(g). Combining P and $\nu_{x/y}$, we can conclude that a SONLS with coexisting first-order flat band, which plays the role of drumhead surface states, and second-order hinge states are formed in our m -parameterized 2D system. The phase diagram of the SONLS in different θ is shown in Fig. 1(h), where the nodal lines exist in the gapless regimes. Our parameter-dimensional SONLS are different from Ref. [51–54] and it refreshes one's general belief that nodal-line semimetals need \mathcal{PT} symmetry or mirror-rotation symmetry [57]. This exotic phase enriches our understanding of 2D topological phase and provides new possibilities for the application of 2D materials in quantum devices.

Besides the SONLS, the flux in our system can also induce the SOTI. When $\theta = \pi$ and $\gamma_x = \gamma_y \equiv \gamma$, the time-reversal $\mathcal{T} = K$, with K being the complex conjugation, the spatial inversion $\mathcal{P} = \tau_0 \sigma_y$, and the mirror-rotation $\mathcal{M}_{xy} = [(\tau_0 + \tau_z)\sigma_x - (\tau_z - \tau_0)\sigma_z]/2$ symmetries are recovered. Its topology is described by $\mathcal{H}(k, k)$ along the high-symmetry line $k_x = k_y \equiv k$, which is diagonalized into $\text{diag}[\mathcal{H}^+(k), \mathcal{H}^-(k)]$ with $\mathcal{H}^\pm(k) = \mathbf{h}^\pm \cdot \boldsymbol{\sigma}$ and $\mathbf{h}^\pm = \sqrt{2}[\gamma + (\lambda + m) \cos k, \pm(\lambda + m) \sin k, 0]$. Thus, the bands coalesce when $|\gamma| = |\lambda + m|$. It exhibits the SOTI characterized by the mirror-graded winding number $W = W_+ - W_-$ [78], where $W_\pm = \frac{i}{2\pi} \int_0^{2\pi} \langle u_\pm(k) | \partial_k | u_\pm(k) \rangle dk$ and $|u_\pm(k)\rangle$ is the eigenstate of $\mathcal{H}^\pm(k)$. The energy spectrum under the open boundary condition in Fig. 2(a) and the probability distribution of the zero-mode states in Fig. 2(b) show that the system has fourfold degenerate corner states signified by $W = -1$ of Fig. 2(c) when $\lambda > \gamma - m$ and $\lambda < -(\gamma + m)$. The phase diagram in Fig. 2(d) verifies that the SOTI is present when $|\gamma| < |\lambda + m|$.

Floquet engineering.—Being determined by the hopping forms on the lattice, neither the topological features nor the nodal-line structure in static systems can be changed anymore once their material samples are fabricated. Without resorting to changing the intrinsic parameters of the materials, we use Floquet engineering to conveniently control the topological features and generate rich nodal-line structures. First, we consider that the Peierls phase θ is periodically driven as

$$\theta(t) = \begin{cases} \theta_1, & t \in [nT, nT + T_1) \\ \theta_2, & t \in [nT + T_1, (n+1)T) \end{cases}, \quad (3)$$

where $n \in \mathbb{Z}$ and $T = T_1 + T_2$ is the driving period. The periodically driven system $\hat{H}(t)$ does not have a well-defined energy spectrum because its energy is not conserved. According to the Floquet theorem, the one-period evolution operator $\hat{U}_T = \mathbb{T}e^{-i \int_0^T \hat{H}(t) dt}$ defines an effective Hamiltonian $\hat{H}_{\text{eff}} = \frac{i}{T} \ln \hat{U}_T$, whose eigenvalues are called quasienergies [79, 80]. The topological feature of our periodic system is defined in the quasienergy spectrum. Applying the Floquet theorem on our system, we

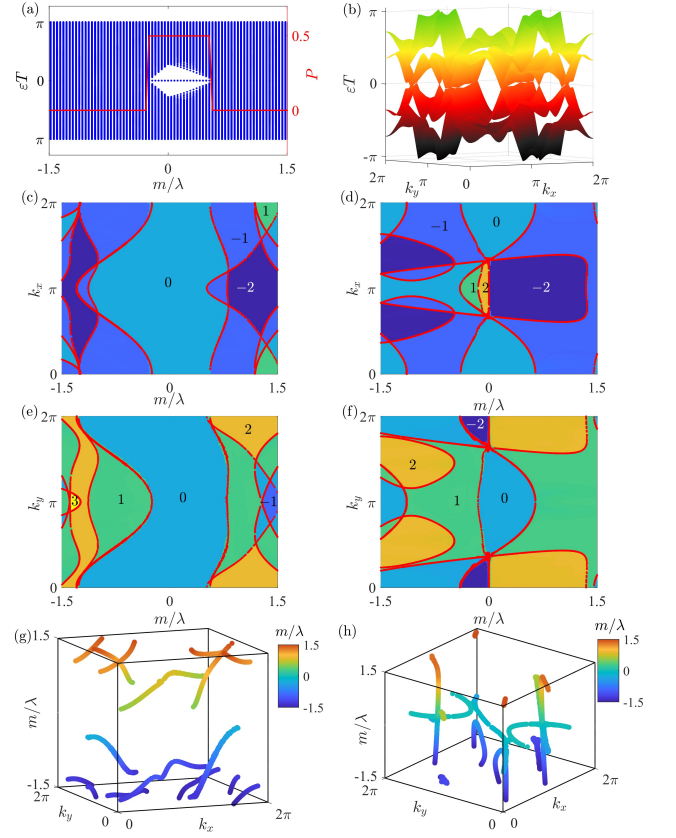


FIG. 3. (a) Quasienergy spectrum and quadrupole moment (red line) of the periodically driven system. (b) Energy spectra in momentum space. Chiral winding numbers (c) ν_y^0 , (d) $\nu_y^{\pi/T}$, (e) ν_x^0 , and (f) $\nu_y^{\pi/T}$ in the k_x - m and k_y - m planes, respectively. Nodal-line distribution of the (e) zero-mode and (f) π/T -mode in the Brillouin zone. We use $\gamma_x = 0.65\lambda$, $\gamma_y = -0.4\lambda$, $\theta_1 = 0$, $\theta_2 = \pi$, $T_1 = \lambda^{-1}$, and $T_2 = 1.5\lambda^{-1}$.

have $\mathcal{H}_{\text{eff}}(\mathbf{k}) = \frac{i}{T} \ln[e^{-i\mathcal{H}_2(\mathbf{k})T_2}e^{-i\mathcal{H}_1(\mathbf{k})T_1}]$, where $\mathcal{H}_j(\mathbf{k})$ is the Hamiltonian with θ replaced by θ_j .

The topological phases of the periodic system are carried by the quasienergy gaps not only at zero but also at π/T [54, 71, 81], which makes the topological description in static systems insufficient. We can establish a complete topological description of our periodic system from $\mathcal{H}_{\text{eff}}(\mathbf{k})$. The first-order topology is described by the winding number, which requires the chiral symmetry. However, $\mathcal{H}_{\text{eff}}(\mathbf{k})$ does not inherit the chiral symmetry of $\mathcal{H}(\mathbf{k})$ due to $[\mathcal{H}_1(\mathbf{k}), \mathcal{H}_2(\mathbf{k})] \neq 0$. We propose to recover the chiral symmetry by making two unitary transformations $G_l(\mathbf{k}) = e^{i(-1)^l \mathcal{H}_l(\mathbf{k})T_l/2}$ ($l = 1, 2$), which do not change the quasienergy spectrum, and obtain $\tilde{\mathcal{H}}_{\text{eff},l}(\mathbf{k}) = iT^{-1} \ln[G_l(\mathbf{k})U_T(\mathbf{k})G_l^\dagger(\mathbf{k})]$. Then two winding numbers ν_l defined in the chirally symmetric $\tilde{\mathcal{H}}_{\text{eff},l}(\mathbf{k})$ can be calculated in the similar manner as Eq. (2). The first-order topology of $\mathcal{H}_{\text{eff}}(\mathbf{k})$ at the quasienergies α/T , with $\alpha = 0$ or π , relates to ν_l as $\nu^\alpha/T = (\nu_1 + e^{i\alpha}\nu_2)/2$ [65]. The number of α/T -mode drumhead surface states

equals to $2|\nu^{\alpha/T}|$. Being same as the static case, the second-order topology is captured by P .

The quasienergy spectrum of $\mathcal{H}_{\text{eff}}(\mathbf{k})$ in Fig. 3(a) shows that the second-order corner states signified by $P = 0.5$ are present at the quasienergy zero. We also find that large parts of the quasienergy gaps at both zero and π/T are closed. Figure 3(b) reveals that the band-touching form becomes more complicated than the static case in Fig. 1(c), which endows us with a sufficient room to adjust the nodal-line structure and the number of the drumhead surface states by Floquet engineering. The winding numbers $\nu_{x/y}^{\alpha/T}$ in Figs. 3(c)-3(f) reveal that the regimes with the closed quasienergy gaps exhibit more colorful first-order topological phases than the static case in Figs. 1(e) and 1(f). In particular, the large-winding-number phases with ν^0 from -2 to 3 and $\nu^{\pi/T}$ from -2 to 2 absent in the static case are present. Combined with the second-order topological phases in Fig. 3(a), this result demonstrates that a m -parameterized hybrid-order nodal-line semimetal, with coexisting second-order nodal lines in the zero mode and the first-order ones in the π/T mode, are created by the periodic driving. Figures 3(g) and 3(h) show the distribution of the zero- and π/T -mode nodal lines in the m -parameterized Brillouin zone. We see that the nodal-line structures are dramatically changed by the periodic driving compared with the static case in Fig. 1(g). First, the number of zero-mode nodal lines increases. Second, the π/T -mode nodal lines are interwoven to form a nodal net at the $m = 0.1\lambda$ plane and nodal loops at m from -1.5λ to -1.2λ . Such rich nodal-line structures confirms the diverse topological phases in Figs. 3(c)-3(f), which are difficult to realize in static systems. Thus, our result reveals that the periodic driving supplies an efficient tool to adjust the nodal-line structures and the topological phases.

Next, we study the rich SOTI induced by the Floquet engineering by choosing $\gamma_x = \gamma_y$. Setting $\theta = \pi$ to preserve the \mathcal{PT} and mirror-rotation symmetries, the periodic driving is applied on m as

$$m(t) = \begin{cases} m_1, & t \in [nT, nT + T_1) \\ m_2, & t \in [nT + T_1, (n+1)T) \end{cases} \quad (4)$$

$\mathcal{H}_{\text{eff}}(\mathbf{k})$ is derived in the same manner as above. First, the topological description can be established on $\mathcal{H}_{\text{eff}}(\mathbf{k})$. After making two unitary transformations $G_l(\mathbf{k})$ to $\mathcal{H}_{\text{eff}}(\mathbf{k})$ to recover the chiral symmetry, we calculate the winding numbers W_l from $\tilde{\mathcal{H}}_{\text{eff},l}(\mathbf{k})$. The SOTI in the quasienergy gaps α/T are characterized by the mirror-graded winding number $W_{\alpha/T} = (W_1 + e^{i\alpha}W_2)/2$. The number of α/T -mode corner states equals to $4|W_{\alpha/T}|$. Second, it is derived from $\mathcal{H}_{\text{eff}}(\mathbf{k})$ that the phase transition occurs for \mathbf{k} and the parameters satisfying either [65, 71, 81]

$$T_j E_j = c_j \pi, \quad (5)$$

$$\text{or} \quad \begin{cases} \mathbf{h}_1 \cdot \mathbf{h}_2 = \pm 1, \\ T_1 E_1 \pm T_2 E_2 = c\pi, \end{cases} \quad (6)$$

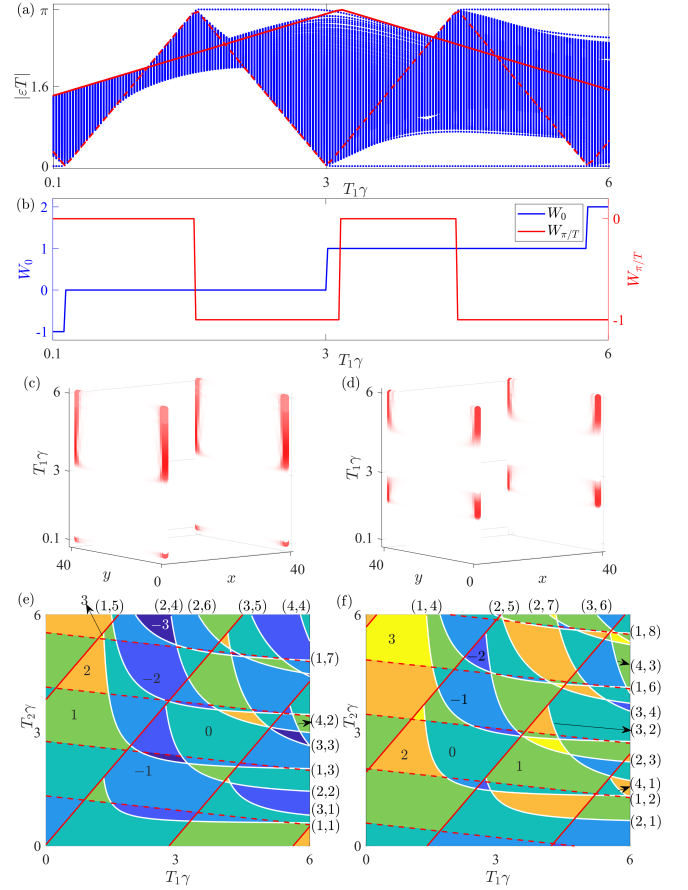


FIG. 4. (a) Quasienergy spectrum and (b) mirror-graded winding number $W_{\alpha/T}$ of the periodically driven system when $T_2 = 0.3\gamma^{-1}$. The red solid (dashed) line is the dispersion relation along the high-symmetry line $k = 0$ (π). Probability distributions of the (c) zero- and (d) π/T -mode states in different T_1 . Phase diagram described by (e) W_0 and (f) $W_{\pi/T}$. The white solid lines are from Eqs. (7) with (c_1, c_2) labeled explicitly. The red solid lines are from Eqs. (8) with $c_{\pi,-} = -2, 0, 2, 4$ in (e), $c_{\pi,-} = -3, -1, 1, 3$ in (f) and red dashed line with $c_{0,+} = 2, 4, 6, 8$ in (e), $c_{0,+} = 1, 3, 5, 7, 9$ in (f). We use $\lambda = 0$, and $m_1 = -0.6\gamma$, $m_2 = 2.2\gamma$.

with $\mathbf{h}_j \equiv \mathbf{h}_j/|\mathbf{h}_j|$, at the quasienergy zero (or π/T) when c_j are integers with same (or different) parity and c is even (or odd) number. Using Eqs. (5) and (6) on $\mathcal{H}^{\pm}(k)$, we obtain the phase boundaries as follows. Equation (5) results in that phase transition occurs at \mathbf{k} satisfying

$$\sqrt{2}[\gamma^2 + (\lambda + m_j)^2 + 2\gamma(\lambda + m_j)\cos k]^{\frac{1}{2}}T_j = c_j\pi. \quad (7)$$

According to Eq. (6), $\mathbf{h}_1 \cdot \mathbf{h}_2 = \pm 1$ needs the high-symmetry line $k \equiv \bar{k} = 0$ or π . Thus, the phase transition occurs at

$$\sqrt{2}[\gamma + (\lambda + m_1)e^{i\bar{k}}T_1 \pm \gamma + (\lambda + m_2)e^{i\bar{k}}T_2] = c_{\bar{k},\pm}\pi. \quad (8)$$

Figures 4(a) and 4(b) show the quasienergy spectrum and mirror-graded winding numbers $W_{\alpha/T}$ of $\mathcal{H}_{\text{eff}}(\mathbf{k})$.

It is seen that the α/T -mode corner states are well described by $W_{\alpha/T}$. Their probability distributions in Figs. 4(c) and 4(d) confirm that SOTI is formed in both the zero and π/T modes. To give a global picture of the SOTI, we plot in Figs. 4(e) and 4(f) the phase diagram characterized by $W_{\alpha/T}$ in the T_2 - T_1 plane. Much richer SOTI with a widely tunable number of zero- and π/T -mode corner states than the static case in Fig. 2(d) are created by the periodic driving. The phase boundaries are well described by the analytical conditions of Eqs. (7) and (8). All the results indicate that periodic driving assisted by the flux offers us a useful way to generate exotic second-order topology phases.

Discussion and conclusion.—Our result is generalizable to the 3D case, where the SONLS can be induced by the flux in the system without mirror-rotation and \mathcal{PT} symmetries. The step-like driving protocol is considered just for the convenience of numerical calculation. Our scheme is generalizable to other driving forms. The second-order semimetals have been predicted in Cd_3As_2 , KMgBi , and PtO_2 [48, 82] and realized in classical acoustic metamaterials [83, 84]. The SOTI have been realized in various systems [85–91]. Floquet engineering has been used to design novel topological phases in several platforms [61, 92–98]. The progress indicates that our result is realizable in the state-of-the-art experiments.

In summary, we have proposed a flux-induced novel parameter-dimensional SONLS in a system without \mathcal{PT} and mirror-rotation symmetries. It enriches our understanding of 2D topological phase and provides new possibilities for the application of 2D materials. Then we found that an exotic hybrid-order nodal-line semimetal and abundant nodal-line structures are created at ease by the periodic driving. We have also discovered a flux-induced SOTI and explored the its wide tunability by Floquet engineering. Our work enriches the family of topological semimetals and provides a convenient way to reduce the practical difficulties in adjusting the nodal line structures, the Fermi arcs, drumhead surface states of SONLS, and the numbers of the corner states of SOTI in static systems. This significantly expands the application of topological materials and enriches their controllability.

Acknowledgments.—The work is supported by the National Natural Science Foundation (Grants No. 12275109, No. 12247101, and No. 11834005).

* anjhong@lzu.edu.cn

- [1] M. Z. Hasan and C. L. Kane, Colloquium: Topological insulators, *Rev. Mod. Phys.* **82**, 3045 (2010).
- [2] X.-L. Qi and S.-C. Zhang, Topological insulators and superconductors, *Rev. Mod. Phys.* **83**, 1057 (2011).
- [3] C.-K. Chiu, J. C. Y. Teo, A. P. Schnyder, and S. Ryu, Classification of topological quantum matter with symmetries, *Rev. Mod. Phys.* **88**, 035005 (2016).
- [4] N. P. Armitage, E. J. Mele, and A. Vishwanath, Weyl and Dirac semimetals in three-dimensional solids, *Rev. Mod. Phys.* **90**, 015001 (2018).
- [5] B. Q. Lv, T. Qian, and H. Ding, Experimental perspective on three-dimensional topological semimetals, *Rev. Mod. Phys.* **93**, 025002 (2021).
- [6] Z. K. Liu, B. Zhou, Y. Zhang, Z. J. Wang, H. M. Weng, D. Prabhakaran, S.-K. Mo, Z. X. Shen, Z. Fang, X. Dai, Z. Hussain, and Y. L. Chen, Discovery of a three-dimensional topological Dirac semimetal, Na_3Bi , *Science* **343**, 864 (2014).
- [7] M. Neupane, S.-Y. Xu, R. Sankar, N. Alidoust, G. Bian, C. Liu, I. Belopolski, T.-R. Chang, H.-T. Jeng, H. Lin, A. Bansil, F. Chou, and M. Z. Hasan, Observation of a three-dimensional topological Dirac semimetal phase in high-mobility Cd_3As_2 , *Nat. Commun.* **5**, 3786 (2014).
- [8] S. Borisenko, Q. Gibson, D. Evtushinsky, V. Zabolotnyy, B. Büchner, and R. J. Cava, Experimental realization of a three-dimensional Dirac semimetal, *Phys. Rev. Lett.* **113**, 027603 (2014).
- [9] S.-Y. Xu, C. Liu, S. K. Kushwaha, R. Sankar, J. W. Krizan, I. Belopolski, M. Neupane, G. Bian, N. Alidoust, T.-R. Chang, H.-T. Jeng, C.-Y. Huang, W.-F. Tsai, H. Lin, P. P. Shibayev, F.-C. Chou, R. J. Cava, and M. Z. Hasan, Observation of Fermi arc surface states in a topological metal, *Science* **347**, 294 (2015).
- [10] S. M. Young, S. Zaheer, J. C. Y. Teo, C. L. Kane, E. J. Mele, and A. M. Rappe, Dirac semimetal in three dimensions, *Phys. Rev. Lett.* **108**, 140405 (2012).
- [11] R. Y. Chen, Z. G. Chen, X.-Y. Song, J. A. Schneeloch, G. D. Gu, F. Wang, and N. L. Wang, Magnetoinfrared spectroscopy of Landau levels and Zeeman splitting of three-dimensional massless Dirac fermions in ZrTe_5 , *Phys. Rev. Lett.* **115**, 176404 (2015).
- [12] Y. Liu, X. Yuan, C. Zhang, Z. Jin, A. Narayan, C. Luo, Z. Chen, L. Yang, J. Zou, X. Wu, S. Sanvito, Z. Xia, L. Li, Z. Wang, and F. Xiu, Zeeman splitting and dynamical mass generation in Dirac semimetal ZrTe_5 , *Nat. Commun.* **7**, 12516 (2016).
- [13] S. M. Young and C. L. Kane, Dirac semimetals in two dimensions, *Phys. Rev. Lett.* **115**, 126803 (2015).
- [14] T.-R. Chang, S.-Y. Xu, D. S. Sanchez, W.-F. Tsai, S.-M. Huang, G. Chang, C.-H. Hsu, G. Bian, I. Belopolski, Z.-M. Yu, S. A. Yang, T. Neupert, H.-T. Jeng, H. Lin, and M. Z. Hasan, Type-II symmetry-protected topological Dirac semimetals, *Phys. Rev. Lett.* **119**, 026404 (2017).
- [15] X. Wan, A. M. Turner, A. Vishwanath, and S. Y. Savrasov, Topological semimetal and Fermi-arc surface states in the electronic structure of pyrochlore iridates, *Phys. Rev. B* **83**, 205101 (2011).
- [16] S.-Y. Xu, I. Belopolski, N. Alidoust, M. Neupane, G. Bian, C. Zhang, R. Sankar, G. Chang, Z. Yuan, C.-C. Lee, S.-M. Huang, H. Zheng, J. Ma, D. S. Sanchez, B. Wang, A. Bansil, F. Chou, P. P. Shibayev, H. Lin, S. Jia, and M. Z. Hasan, Discovery of a Weyl fermion semimetal and topological Fermi arcs, *Science* **349**, 613 (2015).
- [17] B. Q. Lv, H. M. Weng, B. B. Fu, X. P. Wang, H. Miao, J. Ma, P. Richard, X. C. Huang, L. X. Zhao, G. F. Chen, Z. Fang, X. Dai, T. Qian, and H. Ding, Experimental discovery of Weyl semimetal TaAs , *Phys. Rev. X* **5**, 031013 (2015).
- [18] X. Huang, L. Zhao, Y. Long, P. Wang, D. Chen, Z. Yang, H. Liang, M. Xue, H. Weng, Z. Fang, X. Dai, and

- G. Chen, Observation of the Chiral-Anomaly-Induced negative magnetoresistance in 3D Weyl semimetal TaAs, *Phys. Rev. X* **5**, 031023 (2015).
- [19] T. Nguyen, F. Han, N. Andrejevic, R. Pablo-Pedro, A. Apte, Y. Tsurimaki, Z. Ding, K. Zhang, A. Alatas, E. E. Alp, S. Chi, J. Fernandez-Baca, M. Matsuda, D. A. Tennant, Y. Zhao, Z. Xu, J. W. Lynn, S. Huang, and M. Li, Topological singularity induced Chiral Kohn Anomaly in a Weyl semimetal, *Phys. Rev. Lett.* **124**, 236401 (2020).
- [20] S.-M. Huang, S.-Y. Xu, I. Belopolski, C.-C. Lee, G. Chang, B. Wang, N. Alidoust, G. Bian, M. Neupane, C. Zhang, S. Jia, A. Bansil, H. Lin, and M. Z. Hasan, A Weyl Fermion semimetal with surface Fermi arcs in the transition metal monpnictide TaAs class, *Nat. Commun.* **6**, 7373 (2015).
- [21] L. X. Yang, Z. K. Liu, Y. Sun, H. Peng, H. F. Yang, T. Zhang, B. Zhou, Y. Zhang, Y. F. Guo, M. Rahn, D. Prabhakaran, Z. Hussain, S. K. Mo, C. Felser, B. Yan, and Y. L. Chen, Weyl semimetal phase in the non-centrosymmetric compound TaAs, *Nat. Phys.* **11**, 728 (2015).
- [22] C. Shekhar, A. K. Nayak, Y. Sun, M. Schmidt, M. Nicklas, I. Leermakers, U. Zeitler, Y. Skourski, J. Wosnitza, Z. Liu, Y. Chen, W. Schnelle, H. Borrmann, Y. Grin, C. Felser, and B. Yan, Extremely large magnetoresistance and ultrahigh mobility in the topological Weyl semimetal candidate NbP, *Nat. Phys.* **11**, 645 (2015).
- [23] S.-Y. Xu, N. Alidoust, I. Belopolski, Z. Yuan, G. Bian, T.-R. Chang, H. Zheng, V. N. Strocov, D. S. Sanchez, G. Chang, C. Zhang, D. Mou, Y. Wu, L. Huang, C.-C. Lee, S.-M. Huang, B. Wang, A. Bansil, H.-T. Jeng, T. Neupert, A. Kaminski, H. Lin, S. Jia, and M. Zahid Hasan, Discovery of a Weyl fermion state with Fermi arcs in niobium arsenide, *Nat. Phys.* **11**, 748 (2015).
- [24] Z. Yan, R. Bi, H. Shen, L. Lu, S.-C. Zhang, and Z. Wang, Nodal-link semimetals, *Phys. Rev. B* **96**, 041103 (2017).
- [25] C. Li, C. M. Wang, B. Wan, X. Wan, H.-Z. Lu, and X. C. Xie, Rules for phase shifts of quantum oscillations in topological nodal-line semimetals, *Phys. Rev. Lett.* **120**, 146602 (2018).
- [26] N. Xu, Y. T. Qian, Q. S. Wu, G. Autès, C. E. Matt, B. Q. Lv, M. Y. Yao, V. N. Strocov, E. Pomjakushina, K. Conder, N. C. Plumb, M. Radovic, O. V. Yazyev, T. Qian, H. Ding, J. Mesot, and M. Shi, Trivial topological phase of CaAgP and the topological nodal-line transition in CaAg(P_{1-x}As_x), *Phys. Rev. B* **97**, 161111 (2018).
- [27] G. Bian, T.-R. Chang, H. Zheng, S. Velury, S.-Y. Xu, T. Neupert, C.-K. Chiu, S.-M. Huang, D. S. Sanchez, I. Belopolski, N. Alidoust, P.-J. Chen, G. Chang, A. Bansil, H.-T. Jeng, H. Lin, and M. Z. Hasan, Drumhead surface states and topological nodal-line fermions in TlTaSe₂, *Phys. Rev. B* **93**, 121113 (2016).
- [28] R. Yu, H. Weng, Z. Fang, X. Dai, and X. Hu, Topological node-line semimetal and dirac semimetal state in antiperovskite Cu₃PdN, *Phys. Rev. Lett.* **115**, 036807 (2015).
- [29] Y.-H. Chan, C.-K. Chiu, M. Y. Chou, and A. P. Schnyder, Ca₃P₂ and other topological semimetals with line nodes and drumhead surface states, *Phys. Rev. B* **93**, 205132 (2016).
- [30] S. Jia, S.-Y. Xu, and M. Z. Hasan, Weyl semimetals, fermi arcs and chiral anomalies, *Nature Materials* **15**, 1140 (2016).
- [31] C. R. Rajamathi, U. Gupta, N. Kumar, H. Yang, Y. Sun, V. Süß, C. Shekhar, M. Schmidt, H. Blumtritt, P. Werner, B. Yan, S. Parkin, C. Felser, and C. N. R. Rao, Weyl semimetals as hydrogen evolution catalysts, *Advanced Materials* **29**, 1606202 (2017).
- [32] Q. Wang, C.-Z. Li, S. Ge, J.-G. Li, W. Lu, J. Lai, X. Liu, J. Ma, D.-P. Yu, Z.-M. Liao, and D. Sun, Ultrafast broadband photodetectors based on three-dimensional dirac semimetal cd₃as₂, *Nano Lett.* **17**, 834 (2017).
- [33] F. Han, N. Andrejevic, T. Nguyen, V. Kozii, Q. T. Nguyen, T. Hogan, Z. Ding, R. Pablo-Pedro, S. Parjan, B. Skinner, A. Alatas, E. Alp, S. Chi, J. Fernandez-Baca, S. Huang, L. Fu, and M. Li, Quantized thermoelectric hall effect induces giant power factor in a topological semimetal, *Nat. Commun.* **11**, 6167 (2020).
- [34] B. Feng, R.-W. Zhang, Y. Feng, B. Fu, S. Wu, K. Miyamoto, S. He, L. Chen, K. Wu, K. Shimada, T. Okuda, and Y. Yao, Discovery of Weyl nodal lines in a single-layer ferromagnet, *Phys. Rev. Lett.* **123**, 116401 (2019).
- [35] B. Feng, B. Fu, S. Kasamatsu, S. Ito, P. Cheng, C.-C. Liu, Y. Feng, S. Wu, S. K. Mahatha, P. Sheverdyayeva, P. Moras, M. Arita, O. Sugino, T.-C. Chiang, K. Shimada, K. Miyamoto, T. Okuda, K. Wu, L. Chen, Y. Yao, and I. Matsuda, Experimental realization of two-dimensional Dirac nodal line fermions in monolayer Cu₂Si, *Nat. Commun.* **8**, 1007 (2017).
- [36] B. Guo, W. Miao, V. Huang, A. C. Lygo, X. Dai, and S. Stemmer, Zeeman field-induced two-dimensional Weyl semimetal phase in Cadmium Arsenide, *Phys. Rev. Lett.* **131**, 046601 (2023).
- [37] W. A. Benalcazar, B. A. Bernevig, and T. L. Hughes, Quantized electric multipole insulators, *Science* **357**, 61 (2017).
- [38] J. Langbehn, Y. Peng, L. Trifunovic, F. von Oppen, and P. W. Brouwer, Reflection-Symmetric second-order topological insulators and superconductors, *Phys. Rev. Lett.* **119**, 246401 (2017).
- [39] Z. Song, Z. Fang, and C. Fang, ($d - 2$)-dimensional edge states of rotation symmetry protected topological states, *Phys. Rev. Lett.* **119**, 246402 (2017).
- [40] Z. Yan, F. Song, and Z. Wang, Majorana corner modes in a high-temperature platform, *Phys. Rev. Lett.* **121**, 096803 (2018).
- [41] M. Ezawa, Topological switch between second-order topological insulators and topological crystalline insulators, *Phys. Rev. Lett.* **121**, 116801 (2018).
- [42] F. Liu, H.-Y. Deng, and K. Wakabayashi, Helical topological edge states in a quadrupole phase, *Phys. Rev. Lett.* **122**, 086804 (2019).
- [43] R.-X. Zhang, W. S. Cole, X. Wu, and S. Das Sarma, Higher-order topology and nodal topological superconductivity in Fe(Se,Te) heterostructures, *Phys. Rev. Lett.* **123**, 167001 (2019).
- [44] M. J. Park, Y. Kim, G. Y. Cho, and S. Lee, Higher-order topological insulator in twisted bilayer graphene, *Phys. Rev. Lett.* **123**, 216803 (2019).
- [45] X.-L. Sheng, C. Chen, H. Liu, Z. Chen, Z.-M. Yu, Y. X. Zhao, and S. A. Yang, Two-dimensional second-order topological insulator in graphdiyne, *Phys. Rev. Lett.* **123**, 256402 (2019).
- [46] A. Tiwari, M.-H. Li, B. A. Bernevig, T. Neupert, and S. A. Parameswaran, Unhinging the surfaces of higher-order topological insulators and superconductors, *Phys.*

- Rev. Lett. **124**, 046801 (2020).
- [47] Y. Ren, Z. Qiao, and Q. Niu, Engineering corner states from two-dimensional topological insulators, *Phys. Rev. Lett.* **124**, 166804 (2020).
 - [48] B. J. Wieder, Z. Wang, J. Cano, X. Dai, L. M. Schoop, B. Bradlyn, and B. A. Bernevig, Strong and fragile topological Dirac semimetals with higher-order Fermi arcs, *Nat. Commun.* **11**, 627 (2020).
 - [49] H.-X. Wang, Z.-K. Lin, B. Jiang, G.-Y. Guo, and J.-H. Jiang, Higher-order Weyl semimetals, *Phys. Rev. Lett.* **125**, 146401 (2020).
 - [50] S. A. A. Ghorashi, T. Li, and T. L. Hughes, Higher-order Weyl semimetals, *Phys. Rev. Lett.* **125**, 266804 (2020).
 - [51] K. Wang, J.-X. Dai, L. B. Shao, S. A. Yang, and Y. X. Zhao, Boundary criticality of \mathcal{PT} -invariant topology and second-order nodal-line semimetals, *Phys. Rev. Lett.* **125**, 126403 (2020).
 - [52] L. B. Shao, Q. Liu, R. Xiao, S. A. Yang, and Y. X. Zhao, Gauge-field extended $k \cdot p$ method and novel topological phases, *Phys. Rev. Lett.* **127**, 076401 (2021).
 - [53] C. Chen, X.-T. Zeng, Z. Chen, Y. X. Zhao, X.-L. Sheng, and S. A. Yang, Second-order real nodal-line semimetal in three-dimensional graphdiyne, *Phys. Rev. Lett.* **128**, 026405 (2022).
 - [54] M.-J. Gao, H. Wu, and J.-H. An, Engineering second-order nodal-line semimetals by breaking \mathcal{PT} symmetry and periodic driving, *Phys. Rev. B* **107**, 035128 (2023).
 - [55] F. Schindler, A. M. Cook, M. G. Vergniory, Z. Wang, S. S. P. Parkin, B. A. Bernevig, and T. Neupert, Higher-order topological insulators, *Science Advances* **4**, eaat0346 (2018).
 - [56] W. Zhang, X. Xie, H. Hao, J. Dang, S. Xiao, S. Shi, H. Ni, Z. Niu, C. Wang, K. Jin, X. Zhang, and X. Xu, Low-threshold topological nanolasers based on the second-order corner state, *Light. Sci. Appl.* **9**, 109 (2020).
 - [57] J. Li, H. Wang, and H. Pan, Tunable topological phase transition from nodal-line semimetal to Weyl semimetal by breaking symmetry, *Phys. Rev. B* **104**, 235136 (2021).
 - [58] A. Eckardt, Colloquium: Atomic quantum gases in periodically driven optical lattices, *Rev. Mod. Phys.* **89**, 011004 (2017).
 - [59] F. Meinert, M. J. Mark, K. Lauber, A. J. Daley, and H.-C. Nägerl, Floquet engineering of correlated tunneling in the Bose-Hubbard model with ultracold atoms, *Phys. Rev. Lett.* **116**, 205301 (2016).
 - [60] M. C. Rechtsman, J. M. Zeuner, Y. Plotnik, Y. Lumer, D. Podolsky, F. Dreisow, S. Nolte, M. Segev, and A. Szameit, Photonic Floquet topological insulators, *Nature* **496**, 196 (2013).
 - [61] P. Roushan, C. Neill, A. Megrant, Y. Chen, R. Babush, R. Barends, B. Campbell, Z. Chen, B. Chiaro, A. Dunsworth, A. Fowler, E. Jeffrey, J. Kelly, E. Lucero, J. Mutus, P. J. J. O'Huog, Heng, M. Neeley, C. Quintana, D. Sank, A. Vainsencher, J. Wenner, T. White, E. Kapit, H. Neven, and J. Martinis, Chiral ground-state currents of interacting photons in a synthetic magnetic field, *Nat. Phys.* **13**, 146 (2017).
 - [62] T.-S. Xiong, J. Gong, and J.-H. An, Towards large-Chern-number topological phases by periodic quenching, *Phys. Rev. B* **93**, 184306 (2016).
 - [63] H. Liu, T.-S. Xiong, W. Zhang, and J.-H. An, Floquet engineering of exotic topological phases in systems of cold atoms, *Phys. Rev. A* **100**, 023622 (2019).
 - [64] H. Wu and J.-H. An, Floquet topological phases of non-Hermitian systems, *Phys. Rev. B* **102**, 041119 (2020).
 - [65] H. Wu, B.-Q. Wang, and J.-H. An, Floquet second-order topological insulators in non-Hermitian systems, *Phys. Rev. B* **103**, L041115 (2021).
 - [66] L. Li, C. H. Lee, and J. Gong, Realistic Floquet semimetal with exotic topological linkages between arbitrarily many nodal loops, *Phys. Rev. Lett.* **121**, 036401 (2018).
 - [67] Y. Peng and G. Refael, Floquet second-order topological insulators from nonsymmorphic space-time symmetries, *Phys. Rev. Lett.* **123**, 016806 (2019).
 - [68] H. Hu, B. Huang, E. Zhao, and W. V. Liu, Dynamical singularities of Floquet higher-order topological insulators, *Phys. Rev. Lett.* **124**, 057001 (2020).
 - [69] B. Huang and W. V. Liu, Floquet higher-order topological insulators with anomalous dynamical polarization, *Phys. Rev. Lett.* **124**, 216601 (2020).
 - [70] T. Nag, V. Jurić, and B. Roy, Hierarchy of higher-order Floquet topological phases in three dimensions, *Phys. Rev. B* **103**, 115308 (2021).
 - [71] B.-Q. Wang, H. Wu, and J.-H. An, Engineering exotic second-order topological semimetals by periodic driving, *Phys. Rev. B* **104**, 205117 (2021).
 - [72] W. A. Benalcazar, B. A. Bernevig, and T. L. Hughes, Electric multipole moments, topological multipole moment pumping, and chiral hinge states in crystalline insulators, *Phys. Rev. B* **96**, 245115 (2017).
 - [73] C.-A. Li, S.-B. Zhang, J. C. Budich, and B. Trauzettel, Transition from metal to higher-order topological insulator driven by random flux, *Phys. Rev. B* **106**, L081410 (2022).
 - [74] F. D. M. Haldane, Model for a quantum Hall effect without Landau levels: Condensed-matter realization of the "Parity Anomaly", *Phys. Rev. Lett.* **61**, 2015 (1988).
 - [75] B. Kang, K. Shiozaki, and G. Y. Cho, Many-body order parameters for multipoles in solids, *Phys. Rev. B* **100**, 245134 (2019).
 - [76] W. A. Wheeler, L. K. Wagner, and T. L. Hughes, Many-body electric multipole operators in extended systems, *Phys. Rev. B* **100**, 245135 (2019).
 - [77] F. Song, S. Yao, and Z. Wang, Non-Hermitian topological invariants in real space, *Phys. Rev. Lett.* **123**, 246801 (2019).
 - [78] T. Liu, Y.-R. Zhang, Q. Ai, Z. Gong, K. Kawabata, M. Ueda, and F. Nori, Second-order topological phases in non-Hermitian systems, *Phys. Rev. Lett.* **122**, 076801 (2019).
 - [79] H. Sambe, Steady states and quasienergies of a Quantum-Mechanical system in an oscillating field, *Phys. Rev. A* **7**, 2203 (1973).
 - [80] C. Chen, J.-H. An, H.-G. Luo, C. P. Sun, and C. H. Oh, Floquet control of quantum dissipation in spin chains, *Phys. Rev. A* **91**, 052122 (2015).
 - [81] H. Wu and J.-H. An, Non-Hermitian Weyl semimetal and its Floquet engineering, *Phys. Rev. B* **105**, L121113 (2022).
 - [82] C.-Z. Li, A.-Q. Wang, C. Li, W.-Z. Zheng, A. Brinkman, D.-P. Yu, and Z.-M. Liao, Reducing electronic transport dimension to topological hinge states by increasing geometry size of Dirac semimetal Josephson junctions, *Phys. Rev. Lett.* **124**, 156601 (2020).
 - [83] L. Luo, H.-X. Wang, Z.-K. Lin, B. Jiang, Y. Wu, F. Li, and J.-H. Jiang, Observation of a phononic higher-order Weyl semimetal, *Nature Materials* **20**, 794 (2021).

- [84] Q. Wei, X. Zhang, W. Deng, J. Lu, X. Huang, M. Yan, G. Chen, Z. Liu, and S. Jia, Higher-order topological semimetal in acoustic crystals, *Nature Materials* **20**, 812 (2021).
- [85] M. Serra-Garcia, V. Peri, R. Süsstrunk, O. R. Bilal, T. Larsen, L. G. Villanueva, and S. D. Huber, Observation of a phononic quadrupole topological insulator, *Nature* **555**, 342 (2018).
- [86] C. W. Peterson, W. A. Benalcazar, T. L. Hughes, and G. Bahl, A quantized microwave quadrupole insulator with topologically protected corner states, *Nature* **555**, 346 (2018).
- [87] F. Schindler, Z. Wang, M. G. Vergniory, A. M. Cook, A. Murani, S. Sengupta, A. Y. Kasumov, R. Deblock, S. Jeon, I. Drozdov, H. Bouchiat, S. Guéron, A. Yazdani, B. A. Bernevig, and T. Neupert, Higher-order topology in bismuth, *Nat. Phys.* **14**, 918 (2018).
- [88] S. Imhof, C. Berger, F. Bayer, J. Brehm, L. W. Molenkamp, T. Kiessling, F. Schindler, C. H. Lee, M. Greiter, T. Neupert, and R. Thomale, Topoelectrical-circuit realization of topological corner modes, *Nat. Phys.* **14**, 925 (2018).
- [89] H. Fan, B. Xia, L. Tong, S. Zheng, and D. Yu, Elastic higher-order topological insulator with topologically protected corner states, *Phys. Rev. Lett.* **122**, 204301 (2019).
- [90] J. Wu, X. Huang, J. Lu, Y. Wu, W. Deng, F. Li, and Z. Liu, Observation of corner states in second-order topological electric circuits, *Phys. Rev. B* **102**, 104109 (2020).
- [91] S. Mittal, V. V. Orre, G. Zhu, M. A. Gorlach, A. Poddubny, and M. Hafezi, Photonic quadrupole topological phases, *Nature Photonics* **13**, 692 (2019).
- [92] F. Mahmood, C.-K. Chan, Z. Alpichshev, D. Gardner, Y. Lee, P. A. Lee, and N. Gedik, Selective scattering between floquet-bloch and volkov states in a topological insulator, *Nat. Phys.* **12**, 306 (2016).
- [93] J. W. McIver, B. Schulte, F.-U. Stein, T. Matsuyama, G. Jotzu, G. Meier, and A. Cavalleri, Light-induced anomalous Hall effect in graphene, *Nat. Phys.* **16**, 38 (2020).
- [94] K. Wintersperger, C. Braun, F. N. Ünal, A. Eckardt, M. D. Liberto, N. Goldman, I. Bloch, and M. Aidelsburger, Realization of an anomalous Floquet topological system with ultracold atoms, *Nat. Phys.* **16**, 1058 (2020).
- [95] M. C. Rechtsman, J. M. Zeuner, Y. Plotnik, Y. Lumer, D. Podolsky, F. Dreisow, S. Nolte, M. Segev, and A. Szameit, Photonic Floquet topological insulators, *Nature* **496**, 196 (2013).
- [96] S. Mukherjee, A. Spracklen, M. Valiente, E. Andersson, P. Öhberg, N. Goldman, and R. R. Thomson, Experimental observation of anomalous topological edge modes in a slowly driven photonic lattice, *Nat. Commun.* **8**, 13918 (2017).
- [97] L. J. Maczewsky, J. M. Zeuner, S. Nolte, and A. Szameit, Observation of photonic anomalous floquet topological insulators, *Nat. Commun.* **8**, 13756 (2017).
- [98] Q. Cheng, Y. Pan, H. Wang, C. Zhang, D. Yu, A. Gover, H. Zhang, T. Li, L. Zhou, and S. Zhu, Observation of anomalous π modes in photonic Floquet engineering, *Phys. Rev. Lett.* **122**, 173901 (2019).